Marshall Plan Scholarship
Final Report

Understanding Carbide Interactions within F82H Ferritic/Martensitic Steel through Mechanical Spectroscopy

Sebastian Ryan Lam

Department of Nuclear Engineering
University of California, Berkeley

Home Institution Supervisor: Professor Peter Hosemann
Guest Institution Supervisor: Professor Daniel Kiener

Abstract

F82H is being proposed as a structural material for the Japanese breeding blanket design at ITER. The microstructure of F82H is a complex tempered martensitic system making it difficult to identify the individual effects of each microstructure component on the bulk mechanical properties. In this report, we mechanically test F82H before and after a heat treatment to get a more detailled insight on how the nucleation of carbides at different grain boundaries affect mechanical properties. Testing will be done through a novel approach called micromechanical spectroscopy (uMS) which was primarily developed at the Montanuniversitat Leoben and uses microsized cantilever frequency testing to measure energy dissipation properties of the material.

1. Introduction

1.1 A Brief History of Nuclear Power

Fission based nuclear power is an essential part of the global power grid supplying approximately 10% of the world's energy demand. This demand exploded in the 70s and 80s leading to the "nuclear renaissance" of power generation. However this has since plateaued since the 90's due to rising public fears over the technology bolstered by a number of nuclear accidents, associations with nuclear weaponry, and concerns of nuclear waste. The tragic history of nuclear energy has been plagued with accidents, namely Chernobyl (1986) and Fukushima (2011) have tarnished the relations of nuclear energy with the public. Following Chernobyl, polls found that 3 out of every 4 Americans thought living next to a nuclear reactor was highly risky [1]. Still to this day, media portrayal of nuclear power to the public often evokes images of The Incredible Hulk, Godzilla, superpowers, or hydrogen bombs breeding fear into use of the promising technology. Many of the initial nuclear reactors built during the 80s are now reaching their quoted 40 year lifespans leaving many countries with the big question of whether to renew these leases, expand nuclear reactor development, or dismantle the technology entirely. Some countries like Germany have already made the decision to decommission all nuclear plants and decrease reliance on nuclear technology due primarily to public opinions souring.

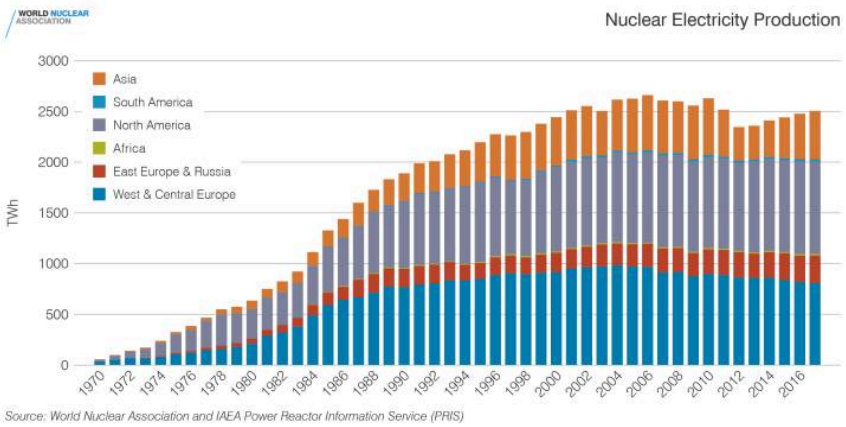

Figure 1. Nuclear electricity production vs time of different countries [2].

This lies in contrast to the general scientific consensus as well as nuclear industry professionals and environmentalists who promote fission based nuclear power as a clean alternative to coal and natural gas which currently powers between 60-80% of the global power grid and emit large amounts of carbon emissions which contribute to the greenhouse effect, accelerating global warming [3]. Since no part of the ideal nuclear fuel cycle involves the production of carbon emissions it has been viewed as a clean carbon energy source to combat global warming. Views of nuclear energy have never been more divided. Advocates see it as a saving grace from the clutches of global warming and critics see it as a vehicle to invisibly poison the public.

The influence of public opinion almost entirely dictates the future of nuclear power due to the poor economics of building a single nuclear reactor. Once built, nuclear reactors are monetarily competitive with their alternatives. However, the astronomical up-front capital expenditure and long construction time frames for a single unit compared to solar and fossil fuel plants make it a risky investment for private companies to develop. It has been decades since the last nuclear reactor started construction in the US and if this trend continues, the industrial knowledge of building reactor components is bound to be lost and become prohibitively expensive to relearn. In the US, you can purchase a home solar system for $10,000 which is a small enough monetary figure to be friendly with investors. For nuclear on the other hand, a power plant with a 1GW capacity is expected to cost somewhere in the ballpark of $6 billion to $15 billion to construct which is extremely risky for even the most speculative of private investment [4]. With this bleak economic situation, public opinion on the technology becomes a heavy influence on the prospects of fission power. Passing bills like carbon taxes, providing subsidies, approving of geological repositories, and increasing speculative investment in nuclear energy are all potential benefits of a positive public perception. This benefit can be seen in the rise of renewable energy sources which experiences massive public approval and governmental subsidies to the point of it being commonplace in many American households. Approval for nuclear power is much higher in the younger generations which might prove to be the light at the end of the tunnel for fission reactors however only time will tell if fission power will thrive or slowly fade away.

This sentiment entirely changes when talking about fusion power which is marketed as the ideal energy source. It’s carbon-emission free, futuristic, powered by water, and the best of all, has (mostly) no radioactivity. Estimates even say that if the entire world was powered off fusion energy, we would have enough fuel to last us longer than predictions for when the Sun would collapse. What is there to hate about infinite, carbon free power? The only problems seem to be that it's still in development and the most promising project, the International Thermonuclear Experimental Reactor (ITER), is heavily over budget and over time [5].

1.2 Fusion Power

Fusion operates on the basic concept of the DT fusion reaction. Deuterium and tritium, both gasses, fuse together in a plasma to form an atom of helium and a neutron with a reaction energy of 17.6MeV [6, 7]. This energy is released entirely to kinetic energy of the helium and neutron atom which can be then absorbed by elastic collisions with a coolant to transfer heat. This heat will then be moved to a steam turbine setup to generate useful electrical energy.

	Thermonuclear Fusion Reaction	Probability	Q MeV
1	${}^{2}_{1}D+{}^{2}_{1}D \rightarrow {}^{3}\mathrm{He} + \mathrm{n}$	50%	3.269
2	${}^{2}_{1}D+{}^{2}_{1}D \rightarrow {}^{3}_{1}T + \mathrm{p}$	50%	4.033
3	${}^{2}_{1}D + {}^{3}_{1}T \rightarrow {}^{4}\mathrm{He} + \mathrm{n}$	100%	17.589
4	${}^{2}_{1}D + {}^{3}\mathrm{He} \rightarrow {}^{4}\mathrm{He} + \mathrm{p}$	100%	18.353
5	${}^{3}_{1}T + {}^{3}_{1}T \rightarrow {}^{4}\mathrm{He} + 2\,\mathrm{n}$	100%	11.332
6	${}^{3}_{1}T + {}^{3}He \rightarrow {}^{2}_{1}D + {}^{4}He$	43%	14.320
7	${}^{3}_{1}T + {}^{3}He \rightarrow p + {}^{5}He$	6%	14.320

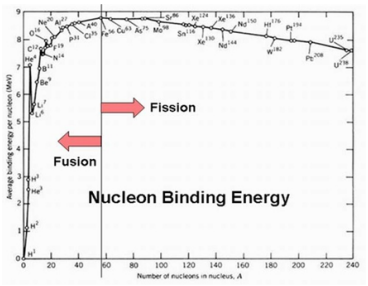

Figure 2. (left) Typical fusion reactions with listed Q value [7]. (right) Nucleon binding energy per nucleon graph [8]

If developed, the benefits of fusion energy over fission energy are immense. Broadly speaking, fission and fusion energy are extremely similar except for the fuel type and nuclear reaction type. Fission energy relies on the fissioning or splitting of uranium or plutonium atoms by neutrons which releases energy. Fusion energy relies on the fusion or smashing together of deuterium or tritium atoms which releases energy. Both reactions generate heat which can then power a steam turbine. Figure 1 shows the basic theory and reactions behind fusion energy [7].

Theoretically getting fusion to work is pretty simple. Just fuse together D-T in some reaction chamber, siphon the heat, boil water, and generate electricity. Modern day hydrogen bombs have been able to take advantage of this same reaction to generate massive amounts of explosive energy, so doing this in a controlled fashion shouldn't be difficult, right? Early scientists thought the exact same thing and early estimates developing fusion energy were placed in the early 90s. Yet, as of today the timeline keeps getting pushed back 10 years and ITER is stated to achieve sustained fusion energy output in 2035. This immense delay in expectations is due to the immense technological challenge that fusion presents. It is often said that ITER is the greatest modern day scientific endeavor of all time and poses a challenge equal to this magnitude. The scientific challenge at ITER is split up into many sectors. Plasma physicists try to find the ideal magnet setup to contain the hot DT plasma, mechanical engineers try to find ideal coolant and flow conditions to maximize heat transfer from the plasma and materials scientists try to find materials which can resist the harsh fusion environment just to say a few [7, 9].

ITER is the biggest attempt being made on an international scale at achieving sustained, controlled fusion energy as a proof of concept for future commercial reactor designs. Many

startups have been developed around the same concept of fusion energy offering a different approach to the challenge however most have ceased operation when initial rounds of investment funding stopped or show little promise for achieving a commercially viable solution to fusion energy.

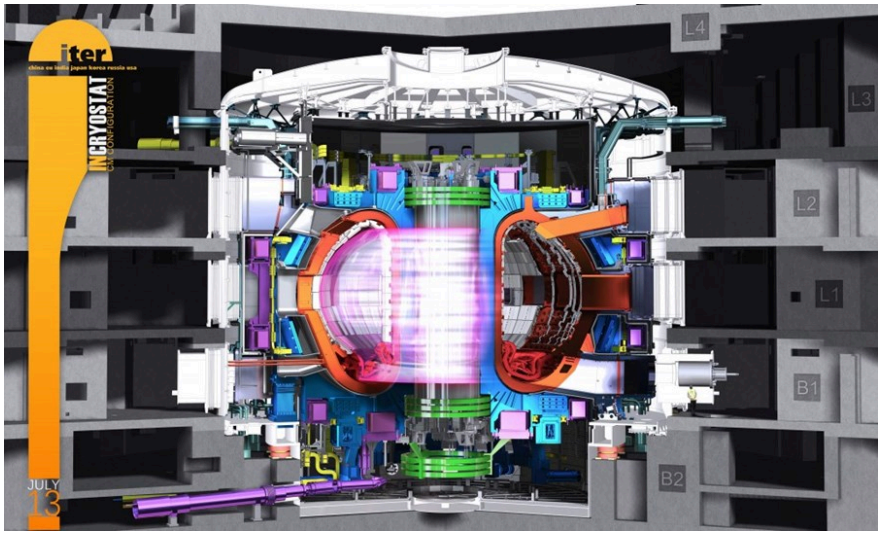

Figure 3. Conceptual design of ITER showing complexity [5].

1.3 Materials Challenge of ITER

The materials challenge at ITER is immense due to the complex environment which is present. The temperature of the plasma is often quoted in excess of 100 million degrees celsius, much hotter than the melting temperature of any known material. While this will be confined by magnets some of this heat will reach the first wall of the vacuum vessel and the material chosen must be able to resist this and transfer this heat to coolant which will in theory spin steam turbines [5, 10]. On top of high temperatures which cause thermal fatigue, expansion, and melting, constant bombardment with 14MeV neutrons and 3.5 MeV helium, geometrical constraints, spallation, neutron activation, coolant flow, magnetic forces, and ease of machining/welding are all concerns for candidate materials. This presents a unique problem in choosing materials which optimize all of these conditions [11].

There are many parts and components for ITER and many collaborating countries have been assigned the task of researching and developing different materials systems for each component [12]. The main component which poses the greatest scientific and engineering challenge is what is called the breeding blanket. The breeding blanket performs many functions and is one probably the biggest design challenge for the entire project. Due to the fact that not enough tritium is naturally available to fuel a fusion reactor due to its short half life, the breeding blanket has to breed tritium within its walls from a neutron reaction with Li-6. It also has to accommodate cooling channels to siphon the heat from the fusion reaction for power generation.

Lastly, it has to withstand the radiation environment and serve as the primary barrier from the fusion reactions and the outside world [7]. With all these functions, many different designs have been proposed ranging from ones using helium as a coolant, water as a coolant, different alloys for the structure, different geometries of the structure, among many other designs. So far, ITER has gone with a shotgun approach, asking every collaborating country to develop their own breeding blanket system using their own alloys and coolant designs.

Japan, a key collaborator in ITER, has the job of developing a water cooled ceramic breeder (WCCB) blanket design .[13–15] Here, they will test the feasibility of using water coolant in the breeding blanket for heat transfer combined with a ceramic LiO_2 pellets which will be used for breeding more tritium. Currently as it stands, work is being done to design and test each country's breeding blanket designs and prototypes where one will be chosen and make it into the final reactor. Following this, Japan's breeding blanket design is still a work in progress and every year their design changes as new simulations and tests are being done to validate its performance. Since the early 1990's ITER has been in its "Basic Performance Phase". This phase has been described as making an initial stage build of the entire tokamak design without any tritium breeding as a proof of concept [16]. Due to the extreme difficulty of the tritium breeding process and the many unknowns of the process, this phase will aim to make a non-sustainable, cheaper version of the reactor to address the main question of whether or not this entire idea is even feasible. As a result of this, it is impossible to know exactly what the newest or best design for the breeding blanket is as it is currently being developed and researched. Every part of the potential breeding blanket design is being constantly iterated upon from the material, geometry, heat transfer properties, among many other factors.

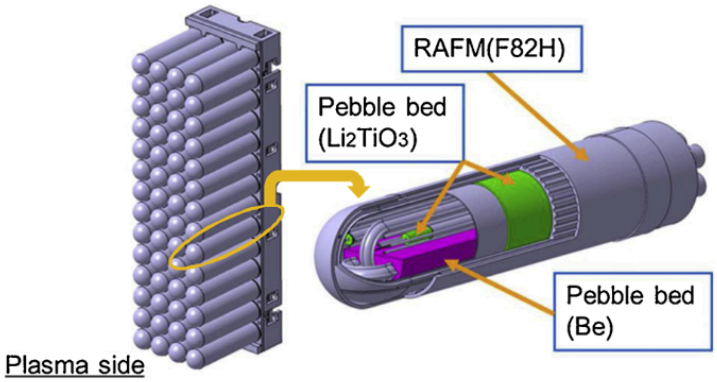

Figure 4. Conceptual design of Japan's test bed module (TBM) for their WCCB design [13].

1.4 Candidate Materials for ITER

The primary challenge for materials selection at ITER is finding materials which are resistant to radiation damage. While other factors like corrosion, magnetic forces, geometrical constraints, and coolant heat transfer are other major issues for ITER, these phenomena have

been well modeled in settings outside fusion energy and knowledge on the subjects are large compared to radiation effects. The effects of radiation on materials is a relatively niche topic which mainly finds applications in advanced semiconductor processes, materials for space travel, fission reactors, and some biological applications. This makes the challenge of high amounts of radiation damage a large unknown for the materials being used for ITER and warrants further study. Due to the immense cost of ITER, combined with the long life expectancies to recoup the large economical investments, this presents a large scientific hurdle for discovering materials which can withstand this environment for decades at a time without replacement. The primary concern with radiation damage is that it has been known to significantly embrittle materials through various mechanisms [17].

Radiation damage occurs in 3 major steps which are vaguely categorized by the time scales in which they happen. For aiding visualization, radiation interaction with materials can be likened to a game of billiards shown in Figure 5. The ball which is hit is an incoming particle of radiation and the material lattice is just a massive array of billiard balls which represent the atoms of the lattice. AS one billiard strikes the rest, it causes a chain reaction, displacing other billiard balls and causing a chaotic collision of billiard balls. Figure 5 shows a demonstration of this concept and shows the results from a single radiation interaction with a lattice. The first step happens immediately as the struck atom is displaced from its initial position creating a vacancy and the ricocheting atom becomes an interstitial within the lattice. This displacement from the original position is the basis for radiation damage which is measured in units of displacements per atom or dpa. The second step is a short term recombination of this displacement damage. More likely than not this initial displacement is “healed” by the displaced atom just popping back into its original position which undos the radiation damage event. This effect is bolstered by increases in temperature, however still a few atoms are permanently displaced from their initial position and are not allowed to recombine. The third step are long term agglomerations of these radiation defects which form structures like stacking fault tetrahedra, dislocation loops, voids, bubbles, and other 2 or 3 dimensional defects which heavily contribute to observed effects of radiation damage in materials. This mechanism forms the basics of the field of nuclear materials with the primary aim is to understand the nature of radiation damage in materials, predict performance of materials in nuclear environments, and create and test materials which are resistant to harsh radiation conditions [17].

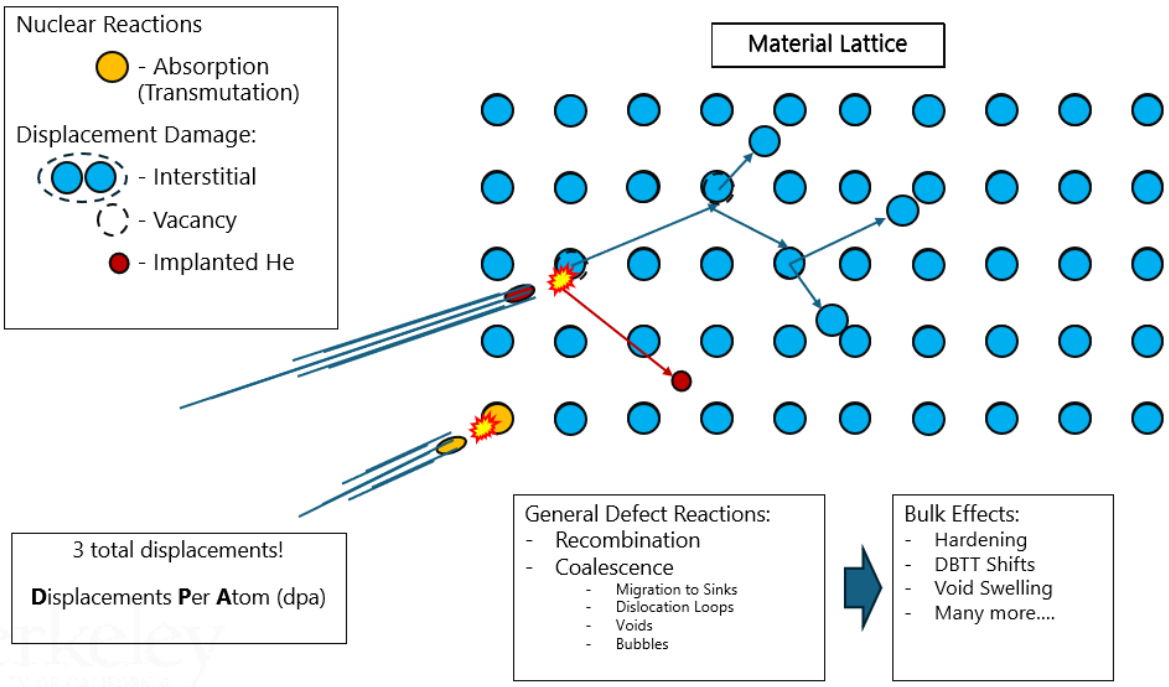

Figure 5. Schematic diagram showing incoming radiation damage and the forms of damage reactions formed.

The effects of radiation on materials have been studied for decades mostly in applications of fission power plants and aerospace applications. While not exactly similar, much of the literature on fission neutron damage in materials can be used to understand which potential materials would perform well in a potential fusion reactor. Early research into fusion reactors primarily used FCC austenitic steels due to their ease of production, machinability, weldability, non-magnetic property, and corrosion resistance. Common types of austenitic steels are usually in the "300 grade" of steels like 304 or 316 which are standard in many applications like cookware, engines, bridges, among many more. However early testing in experimental fusion reactors and fission reactors found that FCC materials perform poorly under an irradiation environment due to their large void swelling. Compared to HCP or BCC steels, FCC steels swell exponentially fast at similar levels of radiation. This can be seen in Figure 6. While this is fine for short term operation, for the 40+ year lifespans of current day fission reactors, this expansion would have increased part dimensions well past tolerances and caused excess stress on adjacent structures leading parts to not fit together anymore. Due to this concern and issues with brittle HCP materials, a shift to studying BCC steels as a structural material was made for fusion applications which are now the most widely accepted material for this application. Initially, BCC steels were not studied due to initial concerns of the magnetic properties of BCC steels interfering with the magnetic coils and fields of the magnetically confined plasma, however modern simulations have been able to address this issue. Currently all the countries who are developing a breeding blanket concept for ITER have adopted use of BCC steels within their

design and most use this as the primary structural material of the breeding blanket. A set of alloys, unique to the fusion materials community, called a reduced activation ferritic/martensitic (RAFM) steels are the most mature structural alloy being considered for fusion applications. Ferritic/martensitic refers to the microstructure of the steel, where a mix of primarily martensite and some ferrite form the BCC structure of the steel. The reduced activation component of RAFM refers to the fact that these alloys were developed with needs to reduce the neutron activation levels of these steels following irradiation [18, 19].

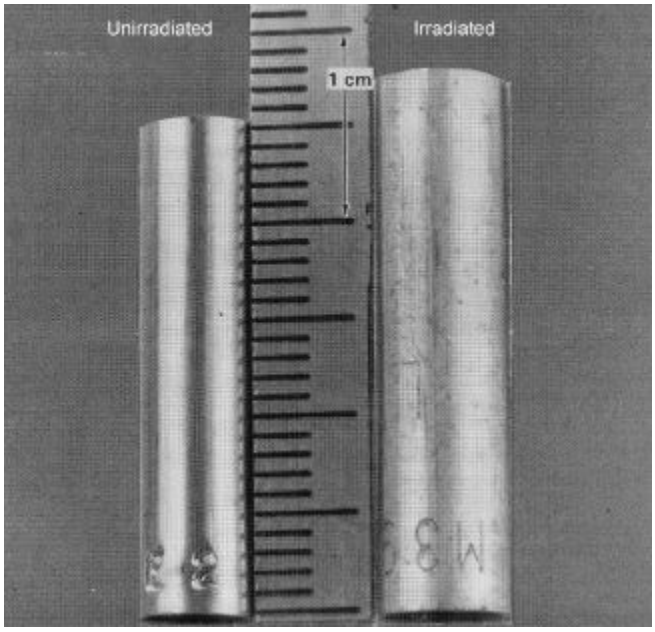

Figure 6 Void swelling induced from irradiation damage showing a large change in sample dimensions [20]

An interesting effect of irradiation, especially from neutrons, is the subsequent activation of whatever material is being irradiated. When a neutron hits the lattice of a material, initially elastic collisions occur causing the radiation damage explained in a previous section. However there is a small chance, which increases as the incoming radiation particle loses energy, of the particle to get absorbed into an atom of the lattice causing inelastic collisions or even absorption. Absorption in this case causes the base atom to transmute into another isotope of the same atom. While this chemically does nothing, this usually leaves the atom in an unstable state where it would want to decay back into a stable state, releasing the excess energy in the form of radiation in the process. The effects of this phenomenon are small compositional changes in irradiated material resulting from the transmutation, and an increase in measured radioactivity of the material. This process is usually described as nuclear activation and has repercussions within fusion reactors. Usually as a result of this process, material properties do not noticeably change

from the small compositional changes resulting from this transmutation and activation. The effects of the elastic collisions and subsequent agglomeration of radiation defects have a much larger influence and cause significant changes to measured material property. However, this phenomenon of activation contributes entirely to the measured radioactivity of materials following irradiation [6].

Radioactivity in the fission process is generated from three main sources: fission products, actinide generation, and nuclear activation of surrounding material. Fission products which dominate short term radioactivity are the resultant nuclei from the fission process which are more often than not highly unstable and thus radioactive. Actinides which dominate long term radioactivity are produced through failed fission reactions where uranium and plutonium end up capturing a neutron, and turning the fissile nuclei to a non-fissile form. This is shown graphically in Figure 7. Nuclear activation is an inherent part of any neutron generating process where neutrons will be captured by surrounding materials (i.e. pipes, the pressure vessel, cladding, bolts) and transmute them into radioactive forms. Commonly this happens in iron based alloys where Fe-56 absorbs two neutrons and becomes the radioactive isotope Fe-58. While radiation and radioactivity when pertaining to nuclear fission are thought of, images of barrels of nuclear waste containers and oozing yellow goo are often conjured. While inaccurate in many regards, these caricatures of real nuclear waste are the major contributors to radiation emission in a fission based nuclear reactor which encapsulate both fission products and radioactive actinides. However, what is often overlooked is the fact that the structural nuclear reactor parts, bolts, screws, tubes, and the reactor pressure vessel (RPV) which are exposed to radiation, often become radioactive through this nuclear activation process and also contribute to radioactivity observed. Especially when decommissioning reactors, the structural materials of the reactor are classified as nuclear waste and need to be properly disposed of. This is usually an overlooked fact in fission based reactors due to the fact that the levels of radioactivity observed from nuclear waste are orders of magnitude higher than that of the activated structural materials. However fusion reactors do not produce any traditional nuclear waste. This can be seen in the nuclear reactions for a fusion process where no part of the fusion cycle consumes or produces any radioactive atoms besides the initial tritium fuel. This means that the only radioactivity concern for fusion reactors comes from the radioactive tritium fuel which is inherent to the fusion process and structural component activation which can be mitigated through engineering specific alloy compositions which are resistant to nuclear activation [6].

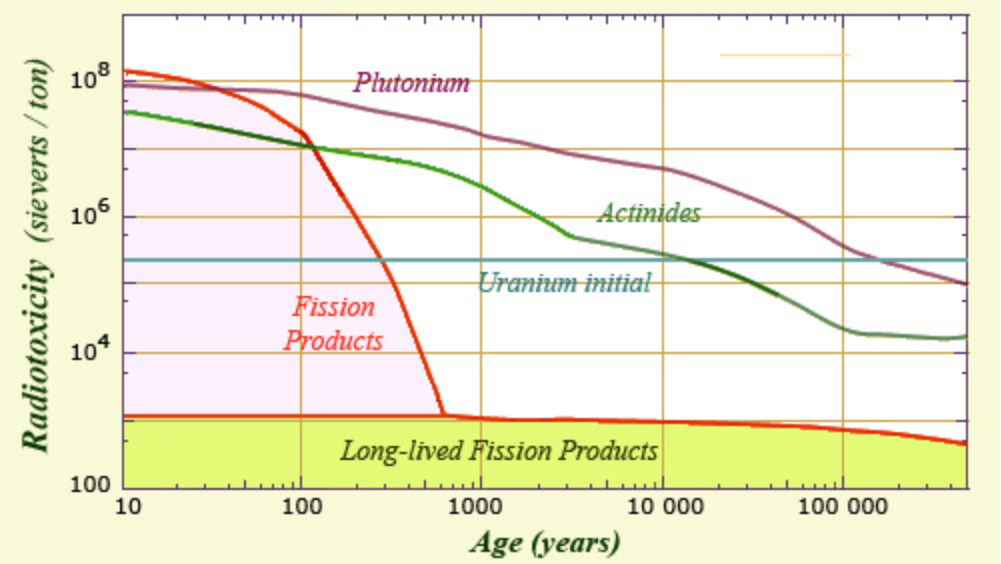

Figure 7. Long lived fission products in typical nuclear waste [21].

There are two primary reasons why there was a large need for the structural materials of a fusion reactor to have a reduced activation component. The first is a public response standpoint, where initial designers wanted to distance fusion energy from the bad reputation of radioactivity. The production of tons of nuclear activated structural materials would not go well for public perception of fusion energy if fears of radioactivity still lingered in the project. The second and more important reason was from an experimental safety standpoint to reduce worker radiation levels. Due to the fact that fusion reactors are still in an experimental phase, much modification is needed with workers constantly removing and adding components. If the entire reactor became activated enough for it to surpass worker yearly radiation dose limits, the entire experiment would either have to be replaced or workers would need to be cycled out on a yearly basis. Either option would be extremely costly, and thus reduced activation components have become integral to the design and function of ITER [19].

1.5 F82H: The Japanese RAFM Steel

The Japanese team of ITER tasked with designing a water cooled ceramic breeder (WCCB) blanket has developed a special RAFM alloy called F82H for their structural material. This alloy with a composition listed in Figure 10. has performed well in studies initially and is similar to many of the other alloys used by other countries. The European team has developed the RAFM alloy EUROFER97 and China has developed RAFM alloy China low activation martensite (CLAM) for their breeder blanket concepts both with very similar compositions to F82H. The microstructure of F82H is described as a tempered martensitic structure. This microstructure is shown in Figure 8.

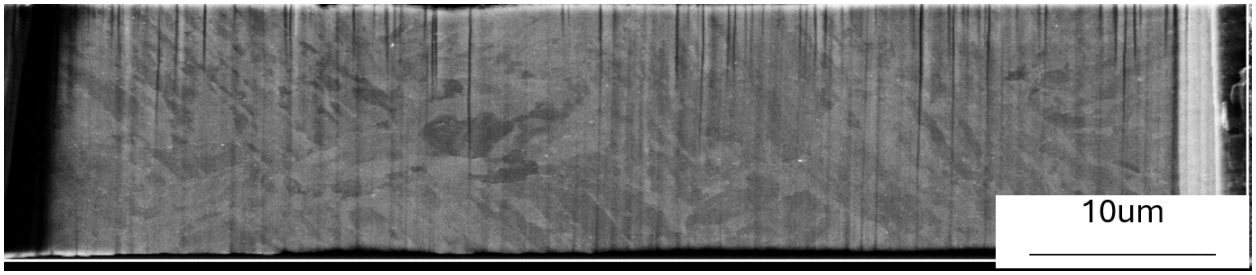

Figure 8. F82H microstructure showing complexity of grains

Martensite is one of the allotropes of iron which is formed upon a rapid diffusionless quench of the alloy. The typical phase diagram for Fe-C is shown in Figure 9. This depicts the major phases of iron including ferrite, cementite, and austenite. At high temperatures and low levels of carbon austenite exists, while at lower temperatures this decomposes into ferrite and cementite phases. Ferrite is an extremely soft allotrope of iron which is composed of almost pure Fe and cementite is an extremely brittle ceramic with a chemical formula of Fe_3C. As a result of this drastic difference in property, most engineering alloys for extreme environments tend to avoid making alloys with just these two allotropes due to poor mechanical and corrosion properties. While this is true for just the plain Fe-C phase diagram, once alloying components like Ni or Co are added, the diagram gets more complicated. Despite austenite being a high temperature phase on the Fe-C phase diagram, it can become stable at room temperature through adding various alloying elements like Ni, Co, or Mn which stabilize the FCC structure of austenite. However after looking at the phase diagram, it is immediately evident that martensite does not form on the equilibrium phase diagram for Fe-C. This is due to the fact that martensite is a metastable phase which isn't thermodynamically favorable. However, if the kinetics of the transition occur in a certain way then martensite can be allowed to form. In Figure . It also shows a time-temperature-transformation (TTT) diagram for a typical steel which shows the formation of martensite. If cooled at a fast enough rate from a high enough temperature, the austenitic phase can rapidly transition to the martensitic phase forming the martensitic structure. Martensite which has just been rapidly cooled, called quenched martensite, is not particularly useful in engineering applications however. Quenched martensite is extremely brittle and shows little toughness behaving close to that of a ceramic with a lower strength, which is not preferred for most applications. This is due to the fast diffusionless quench process which doesn't allow for the carbon atoms in the steel to diffuse into stable positions in the lattice. This causes a great amount of stress on the lattice and excessive lattice distortion which cause this brittle behavior. However, upon tempering the quenched martensite structure in a subsequent heat treatment, much of these carbon atoms are allowed to diffuse to stable positions within the lattice resulting in an overall lattice relaxation effect where these high internal stresses are removed. This process of quenching then subsequent heating produces the tempered martensite structure which is extremely useful and shows great ductility, toughness, and strength and is common in many engineering applications requiring resistance to extreme environments. This microstructure often

does not have as much corrosion resistance as austenitic steels, however it makes up for this in greatly enhanced mechanical properties [22].

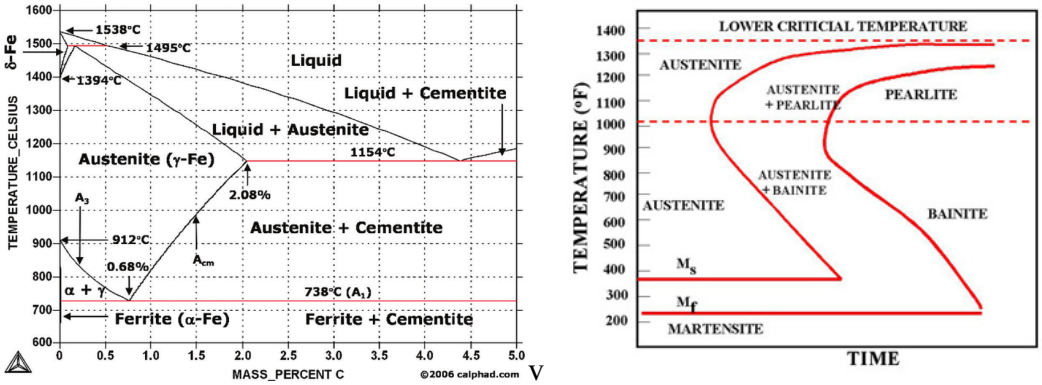

Figure 9. (left) Phase diagram for Fe-C steel. (right) TTT diagram of steel [23, 24]

One unique challenge given to materials scientists looking to develop large-scale fabrication of large structures made of tempered martensitic materials is the fact that high cooling rates are needed for making the alloy. Imagine a hot 1cm cube vs a hot 1m cube being immersed in cold water for the quench. You can imagine that the 1cm cube cools extremely fast, reaching cold temperatures within seconds of immersion in the cold water. However for the hot 1m cube, edges will cool fast, but the core/interior will begin to only slowly cool down. Maybe even after an hour in cold water, the core of the 1m cube will still be hot following the immersion. In these scenarios the 1cm cube would result in a fully transformed martensitic structure while the 1m cube would only have an outer shell of transformed martensite while the interior would be a typical ferrite/cementite mixed microstructure. At first one would think that this issue would rule out martensitic microstructures for the large parts needed at ITER, however material scientists have found that additions of elements like Mo, Nb, and Mn serve to refine grain size and stabilize the martensitic structure. Both of these effects combine to allow for slower cooling rates needed to make a quenched martensite structure which then allows for large components to be made. These elements form the backbone for alloys like T91 or HT9 which already see use in nuclear applications. However, due to the reduced activation needed for F82H, elements like Mo and Nb which heavily activate under neutron irradiation are not optimal for fusion reactor applications like they are for fission applications. After additional testing, Mo and Nb were replaced with W and Ta respectively due to their similar behavior in iron alloys. As they are in the same columns of the periodic table, they should chemically behave similarly which has been validated through experiment. This complex relationship which has been investigated through decades of materials science research has resulted in the final F82H composition listed in Figure 10.

Fe	Cr	W	C	V	Mn	Ta
Bal.	8%	2%	0.1%	0.2	0.1	0.04

Figure 10. F82H nominal composition.

The martensitic structure is complex and is shown in Figure 8 and Figure 11. Here one can see the complex arrangement of parallel grains in block-like formations. This structure is formed as a result of the rapid diffusionless martensitic transformation described in a previous section. The speed and characteristics of this transformation can be elegantly seen in the video: (https://www.youtube.com/watch?v=OQ5lVjYssko) where one can see the rapid nature of the quench and formation of the martensitic grains [25]. The original microstructure starts as an austenitic large grained structure on the order of ~100um per grain. However, upon quenching inside of the large austenitic grain, a fine structure begins to form full of the sharp parallel grains and features which can be seen in the video. This microstructure is typically divided into 4 vague groups of features: prior austenite grains (PAGs), packets, blocks, and laths. Prior austenite grains or PAGs are the grain boundaries forming the largest structure where the large austenite grain was before quenching. Packets are a substructure of a PAG which form large divided sections of parallel sections of the martensitic structure. Blocks are even smaller sub-structures within the packet which form parallel oriented laths. Finally laths are the smallest substructure which are the individual single orientation grains formed in the martensitic transition which are often only 100s of nanometers in diameter. This description vaguely defines the differences in each of the 4 martensitic features which is also displayed in Figure 12 and gives a visual representation.

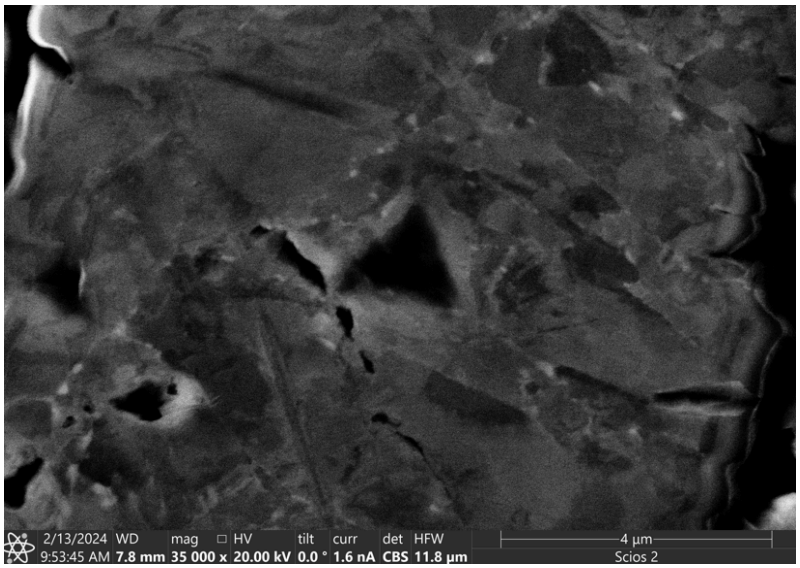

Figure 11. SEM/Electron channeling contrast image (ECCI) of the F82H surface showing complex grains. Triangle in the middle shows a location from nanoindentation testing.

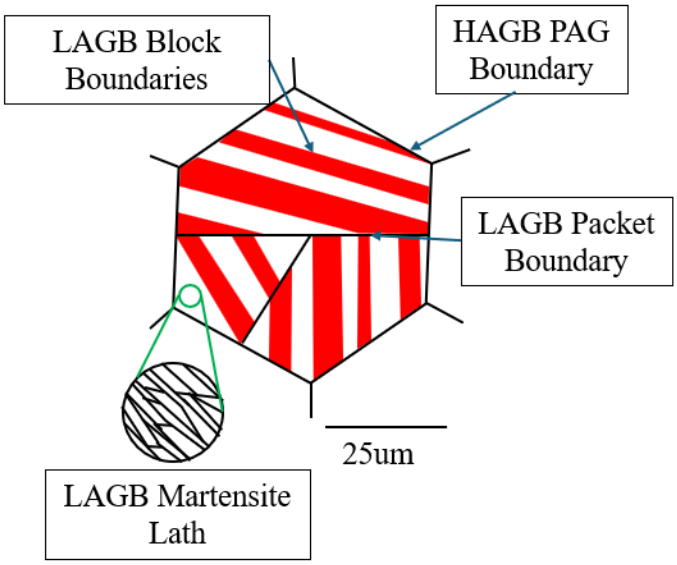

Figure 12. Schematic illustration of the martensite grain structure and substructures.

The tempering procedure serves to increase the toughness of the alloy, however words like toughness and strength used in a materials science setting often describe measurable phenomena or properties. To briefly describe the details of these properties, a basic view of plastic and elastic deformation in materials needs to be understood. Often an analogy with a paperclip is used to describe these phenomena in detail. Let's say you bend a paperclip just a little bit using very little force, what happens following this is that the paperclip immediately bends back to its original shape. This is described as the elastic behavior of a material where, much like an elastic band, the material springs back to its original shape and no damage is done. However, if you instead bend the paperclip using a lot of force, it will instead start to permanently bend. Once you are done bending it, it will not return to its original shape, and is thus permanently deformed also called plastically deformed. This regime of high force describes the permanent or plastic deformation of a material. This basic explanation describes the basics of deformation, however it is also important to understand why this happens. Another useful analogy is thinking of atomic bonds as a series of springs connecting a grid of balls together. The elastic regime is if you start stretching this grid of springs and balls with a low force. At this small force, you are able to bend and stretch this grid of balls however you want, and once you stop applying the force, it is able to spring back to its original position. Plastic deformation on the other hand is like what happens if you stretch this grid of balls and springs so much that the springs start to break and you tear the whole setup apart. While this analogy of springs and balls is a good demonstration for kids, it is not very accurate when analyzing real materials. The primary flaw is that distances between atoms in a real material do not often change by that much upon plastic deformation. The “springs” in this analogy which represent the bonds of atoms do

not often have much “springiness” and will reattach to other atoms once broken off from one. Given this, it doesn’t make too much sense why materials will elongate and change dimensions when given enough force if the bond lengths dont change at all. This means the only other option is that the atoms within the material are physically rearranging themselves as a response to plastic deformation and forces. The reason why a metal gets longer when you apply large forces and stretch it is that planes and rows of atoms are moving through the material lattice and adding extra planes of atoms to the length, making it longer. These extra planes and rows of atoms are called dislocations and are essential to understanding materials deformation. The movement of these dislocations governs all mechanical properties and forms the foundation for why materials deform.

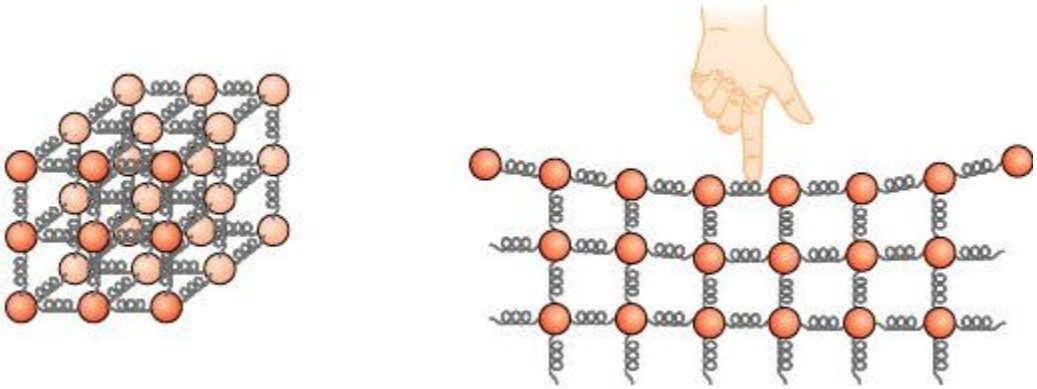

Figure 13 Springs analogy for atoms in a lattice [26].

You can imagine these rows of atoms or dislocations like a line of people holding hands and moving forward together. When this line of people encounter another person or group of people you can imagine that something needs to happen in order for this line of people to pass. Some people might have to unlink their hands to move past the other person or maybe the other person joins the line of people. This basic description is a good analogy for dislocation motion and what happens when they encounter obstacles. As described before, this dislocation movement is essential to deforming a material so any resistance or obstacles to this line of people trying to move forward cause a strengthening effect. When thinking of the word “defect” it's easy to associate this with a flaw or something that has a negative effect on a material, however in the materials science world these defects are often obstacles to dislocation motion which serve to strengthen materials. If there are many obstacles or these defects to impede dislocation motion, then that means that more force is generally needed to overcome these obstacles for dislocations to continue moving, meaning that defects are often correlated with higher forces needed to deform/break a material meaning that it is stronger. In materials there are many types of defects and are often categorized into 4 dimensions: 0D defects are known as point defects which are single point flaws in the lattice like vacancies or interstitials. 1D defects like line defects are primarily composed of dislocations and their different varieties. 2D defects are those like grain boundaries which are planes of atoms which separate regions of aligned atoms. Lastly 3D defects

are those like voids, or alloying elements, inclusions, and dislocation loops which occupy 3 dimensional space and are often large. These four categories of defects all have varying effects on which material is studied, their concentrations, and type and much of materials science is dedicated to studying the effects of these defects not just on mechanical properties, but on electrical, magnetic, and corrosion properties among many others.

During the tempering step following quenching, there are multiple different mechanisms related to the increase in toughness of the alloy. One which was explained before is the relaxation of the internal stresses of the alloy which were created during the metastable positioning of carbon atoms. Another mechanism also mentioned is the subsequent relaxation of lattice distortions caused by the tempering. However, one of the larger effects of the tempering process is the formation of carbides as a result of the increased carbon diffusion during the heat treatment. Carbides are compounds which have the stoichiometry of M_XC_Y where X and Y are integers, M is one of the metal elements in the alloy, and C is carbon. They are formed through the diffusion of carbon atoms during the tempering of the alloy from their metastable positions in the as-quenched condition. This diffusion results in the carbon forming compounds with the alloying metals to form the carbides. The white spots in Figure 11 show these carbides in an F82H sample. These carbides are an integral part of both increasing the toughness, strength and fracture properties of the alloy. One primary mechanism of why is the fact that carbides nucleate primarily on the grain boundaries of the alloy on packet, block, and lath boundaries. The importance of these carbides on grain boundaries has two different effects which contribute to the strength of the alloy. First these carbides serve as greater obstacles to dislocation motion. When dislocations travel through the grain of the material and encounter the grain boundary, the carbides will serve as an additional obstacle on top of the grain boundary to impede dislocation motion and strengthen the material. Second, these carbides also serve as inhibitors to fracture in the material. When materials typically break, this is usually through the propagation of a crack or fracture through the grain of the material. These carbides which are extremely hard serve as sites which will deflect the crack tip to either side, dissipating energy and increasing the fracture toughness of the material. These two primary functions of carbides serve to form the basis for why tempered martensitic steels are so strong and so desired in extreme engineering applications.

In this report, it is our hope to study the intricacies of this carbide strengthening mechanism. Upon tempering we know that these carbides are nucleated on the grain boundaries of F82H and that these carbides will serve to strengthen the material through fracture deflection, forming stress concentrators which will be obstacles to dislocation motion, among other mechanisms. However what is largely not known is 1. Where these carbides will preferentially nucleate and what angle of grain boundary they will prefer and 2. What the effect of these carbides are on the localized mechanical properties of each grain boundary as a function of grain boundary misorientation angle. It is hypothesized that carbides will prefer to nucleate on high angle grain boundaries and will create a greater energy dissipation effect on higher angle grain boundaries which nucleate more carbides. What this would mean for the entire alloy is that lath martensite would form the preferential fracture sites for F82H.

2. Experimental Setup

2.1 The uMS Method

The method which is intended to study the effect of these carbides is through a new technique named micromechanical spectroscopy or uMS. This method was first developed by Dr. Markus Alfrieder at Montanuniversität Leoben, Austria in 2019 uses resonance frequency measurements on cantilevers to sample mechanical properties on a localized scale. This type of testing has been developed before for large cantilevers mostly for applications of coating systems and quantifying coating quality and adhesion. Resonance frequency measurements are also used greatly in a technique called atomic force microscopy (AFM) which uses a cantilever with a pointy tip to tap parts of a sample and develop an extremely detailed map of the surface of a sample. Also the basic mechanical spectroscopy (MS) technique has been in use for decades and used to find energy dissipation mechanisms of largely polymer and amorphous materials. However, uMS makes use of these measurements on a micron scale, using an extremely sensitive testing machine to get nanometer resolution on the movement of microscale cantilevers. With this, materials properties on an extremely small scale can be discovered and fundamentals of energy dissipation mechanisms on select features like individual grain boundaries or grains can be found. To get this data, cantilevers are first fabricated on a micron scale to capture certain grain boundaries or features of interest. Next these cantilevers are then tested using precise equipment which find the resonance frequency of the cantilever. This is done using a materials picoindenter system which has the force and sensitivity needed to deflect these small cantilevers. This machine is set to scan frequency ranges to find that which gives the highest amount of deflection in the cantilevers which forms the resonance frequency of the material. One key note about this process is due to the fact that these resonance frequency measurements often lie at a force low enough to be completely within the elastic regime of the material. This means that the cantilever after testing will be completely undamaged from the process and makes this testing non-destructive in nature. What this means is that the same exact cantilever can be tested following some sort of treatment like a heat treatment or irradiation to get a sense for the effects of some treatment on the mechanical properties and this resonance frequency measurement. This gives uMS the amazing capability to probe the effects of differing treatments on extremely fine features of a material allowing you to have pinpoint accuracy of these effects.

2.2 Cantilever Fabrication

2.2.1 Pre-Prep of the F82H Specimen

A large piece of F82H was procured. In order to make it easier to load this specimen into the testing equipment and to speed up the cantilever fabrication process, a special procedure developed to remove material through polishing, laser cutting, and FIB milling has been used. A specimen of F82H was cut using a combination of a high speed saw with an abrasive SiC cutting wheel and a diamond wire saw into approximately 2mmx3mmx150um pieces. One of these

pieces was then loaded into a custom polishing mount that was used to polish both largest sides of the specimen to a 4000 grit polish. Following this polishing step, one of the sides was chosen to be polished at an approximate 5 degree angle. This created a wedge shape to the specimen which can be seen in Figure 16. Figure 14 shows the special holder and the sample mounted to polish to the 5 degree taper. Due to the low material removal rates of a focused ion beam (FIB) which will be used for the fine sample machining of the final cantilevers, this polished wedge shape which was created is optimal for reducing the total machining time for the FIB. The tip of the edge then was loaded into the femtosecond laser workstation located at MUL to undergo further processing. The home built system operates at a wavelength of 515 nm, pulse duration of 435 fs, a repetition rate of 50kHz, and an average power of 4W. The system was built inside a Zeiss Auriga SEM as a first-of-its-kind processing workstation with parallel fs-laser capabilities with SEM and FIB capabilities. This allows the system to achieve precise laser cuts and rapid examination of the fs-laser ablated area using SEM. The wedge sample of F82H was loaded into the femtosecond laser workstation and the tip of the wedge specimen was laser milled in a pattern shown in figure 16. The reason for this specific design was to reduce time needed when using the FIB to do the fine cutting. This step effectively saves hours of expensive time on the FIB which rates an efficient workflow for making the cantilevers. Images of the final product of the wedge polishing step and the laser processing are shown in figure 15. Figure 16 also shows a schematic diagram of this entire process.

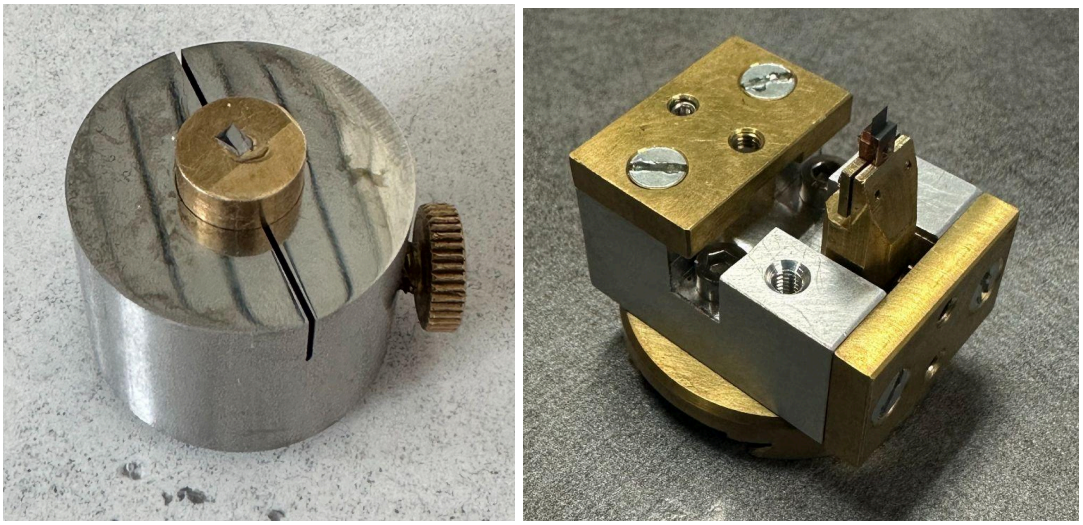

Figure 14. (left) Polishing setup for 5 degree tapered sample wedge. (right) sample mounted in custom holder for FIB milling

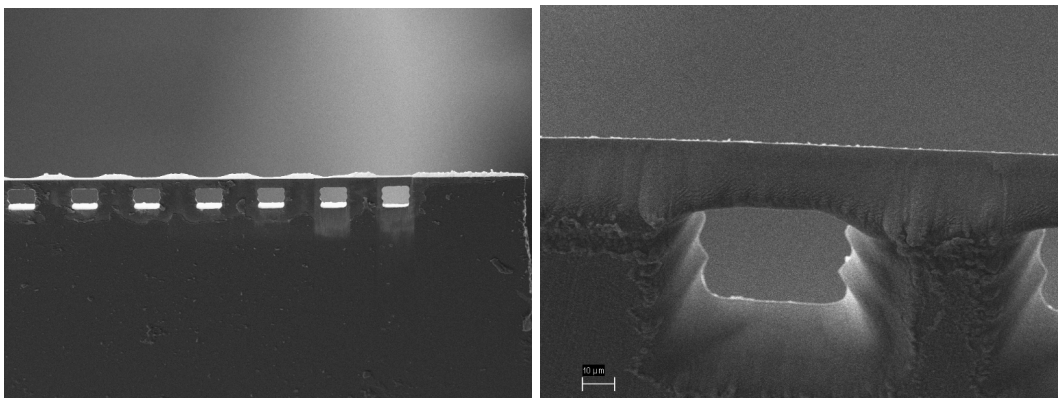

Figure 15. SEM images of the edge of the laser wedge specimen of F82H.

2.2.2 Focused Ion Beam and Backscatter Electron Imaging

Following fs-lasering a FIB was used to do the rest of the milling to shape the cantilever. The wedge specimen was loaded into the special holder shown in Figure 14 which firmly holds the wedge specimen. Figure 17 also shows the wedge holder mounted horizontally being loaded into the SEM. The SEM/FIB used was a X1525 However, due to the need of finding certain grain orientations to machine the cantilevers on, back-scattered electron (BSE) images needed to be taken on the material to identify certain grains which are located in regions representing both lath martensite boundaries and high angle grain boundaries of packet and PAG boundaries. For this, step 3 in Figure 16 shows the procedure where one side of the wedge specimen was FIB milled preliminarily to get an even surface for BSE imaging. Due to the fact that backscattered electrons have a low rate of emission compared to secondary electrons, the detector needed to be extremely close to the sample and the surface of the sample needed to be polished using a low current FIB beam to get the signal necessary for BSE imaging. A total of 15 different sites were prepared like this in order to find grains which were parallel to that of the cantilever direction which are optimal for uMS testing. The surfaces and the resulting BSE images are shown in Figure 18.

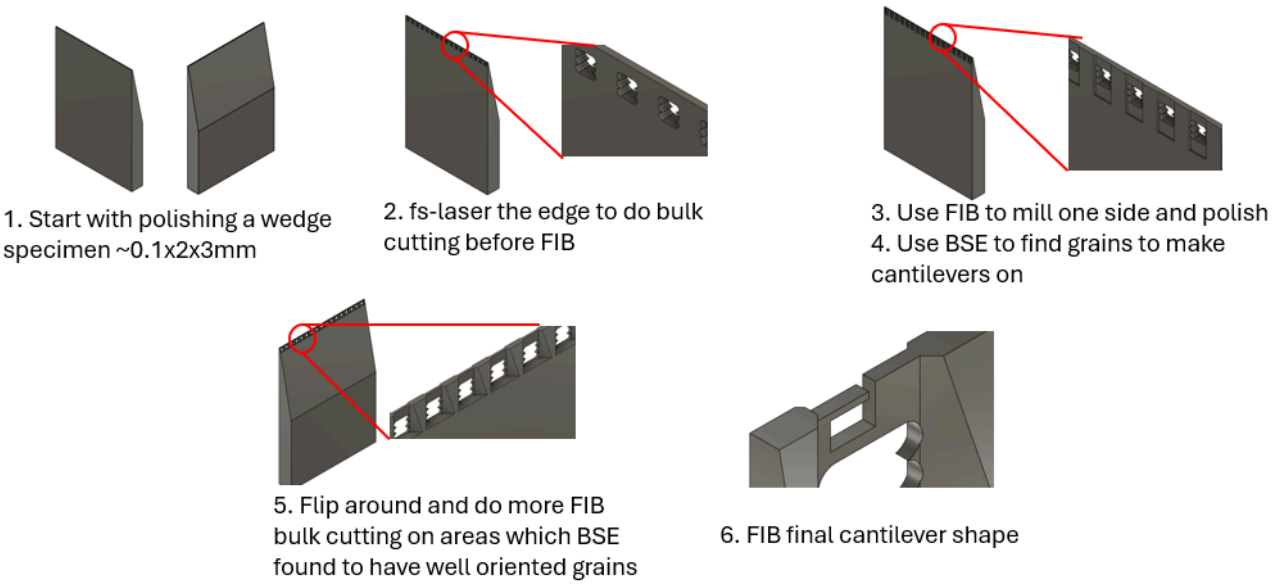

Figure 16. Schematic Diagram of the entire cantilever shaping procedure starting from a wedge specimen.

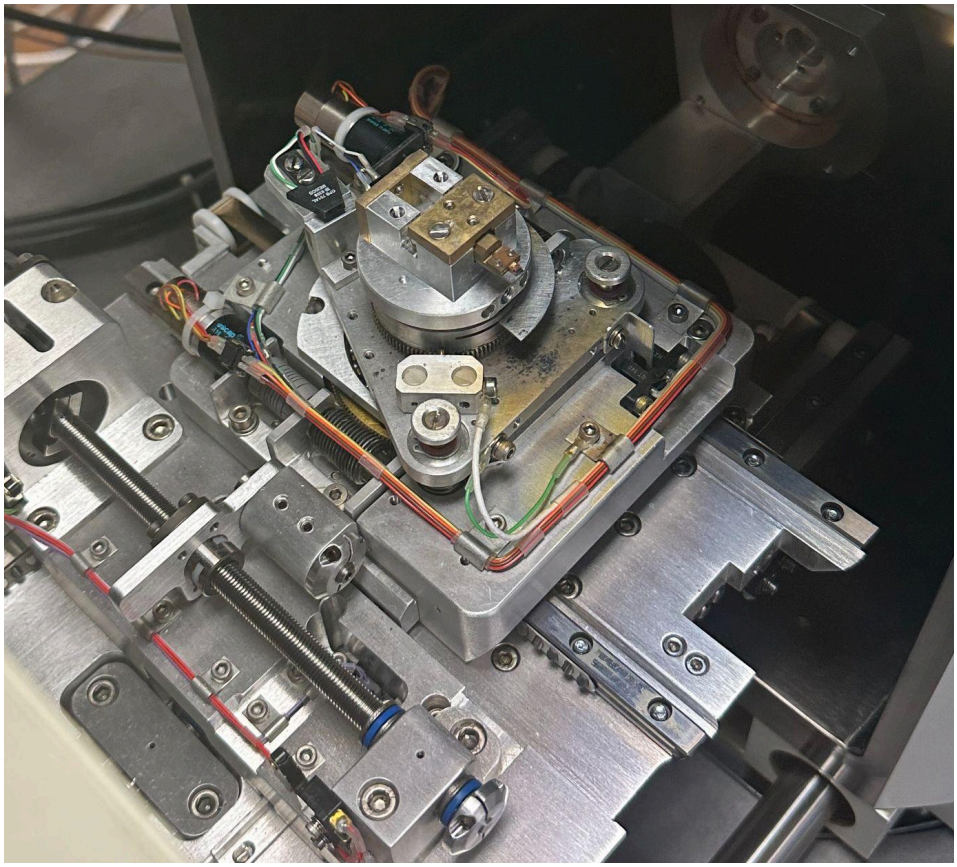

Figure 17. Wedge holder being loaded into SEM for FIB milling and examination

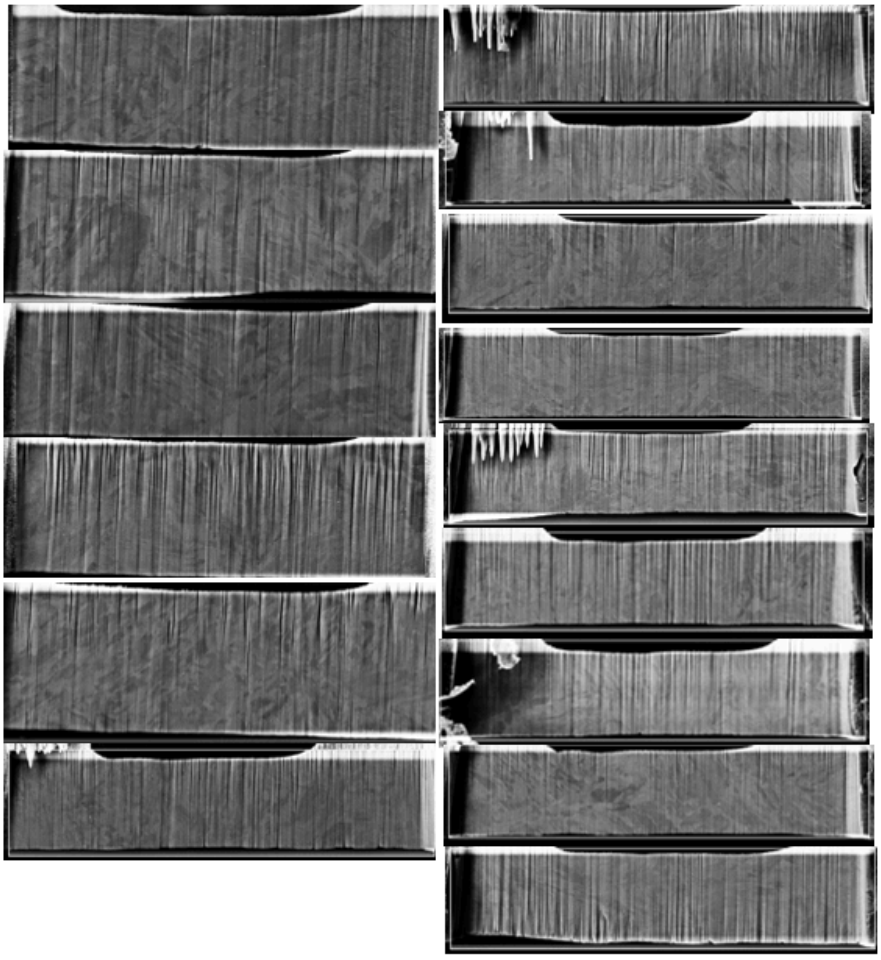

Figure 18. BSE images of each individual site (left) shows Sites 1-6 (right) shows Sites 7-15.

After collecting all the BSE images, a total of 6 different sites looked promising enough in order to pursue making cantilevers on the selected positions. These sites either had parallel oriented grains to the length of the future cantilever, had an approximate 45 degree angle between the grains and the cantilever, or had a large density of fine grained lath martensite. These 6 locations then went through the time consuming process of FIB milling cantilever specimens out of these areas.

FIB milling uses a focused gallion ion beam which is ionized and accelerated toward the sample. This beam can be targeted at certain areas of the sample. When the gallium ions hit the surface of the sample, an elastic collision with the lattice causes atoms of the lattice to sputter off, creating a sort of milling effect similar to that of a sand blaster but at a much smaller scale. The reasons why gallium is commonly chosen for these applications are twofold. One, because gallium has a very low energy needed to ionize and vaporize the metal which can be seen in its low melting point. Two, because gallium is almost never used in real applications. Due to its low

melting point and weak mechanical properties, gallium is almost never used in alloys. This means that the residual gallium which ends up implanting itself in the sample as a result of the gallium ion beam can be almost definitively attributed to the FIB process and not any other external contamination. FIB milling of the final specimen took place in 2 major steps. The first step includes rough cutting of the trenches for the cantilevers. The rough cutting which is shown schematically in Figure 16 is when the sample is thinned to the dimensions of cantilevers. A current of 10nA and an acceleration voltage of 30kV was used to do the rough milling process. Using these parameters, the base shape of the cantilevers were milled to the correct thickness. Pictures of this process are shown in Figure 17 and by the end of the process, a rough shape of the cantilever can be seen.

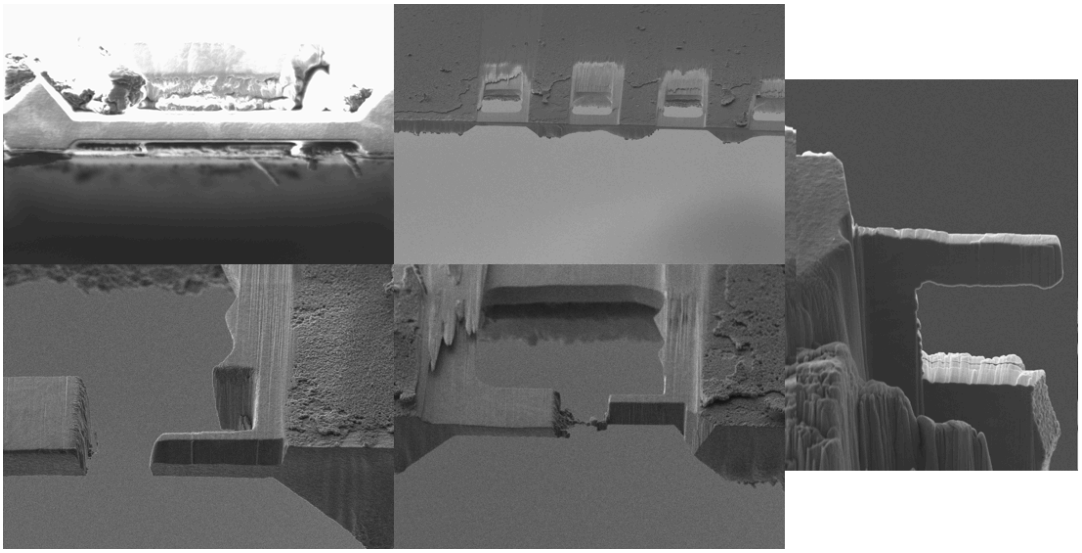

Figure 17. SEM images of the rough FIB milling process at 10nA

Further images of this process for all 6 cantilevers produced can be seen in Figure 18 which outlines the finished rough cutting process. The final cantilever shape can be readily seen here. Following this rough shaping process, the second step in the FIB milling process was performed called fine cutting or polishing. This polishing process is aimed at taking away the stripes or curtaining effects that the rough cutting out onto the sample. At a lower current of 2nA and 30kV voltage, each cantilever was polished using the FIB beam creating a much greater surface finish. Achieving this level of surface is extremely important for the fidelity of the cantilever data since the rough polish leaves a rough surface finish which could serve as unnecessary stress concentrators for mechanical energy giving inconsistent data.

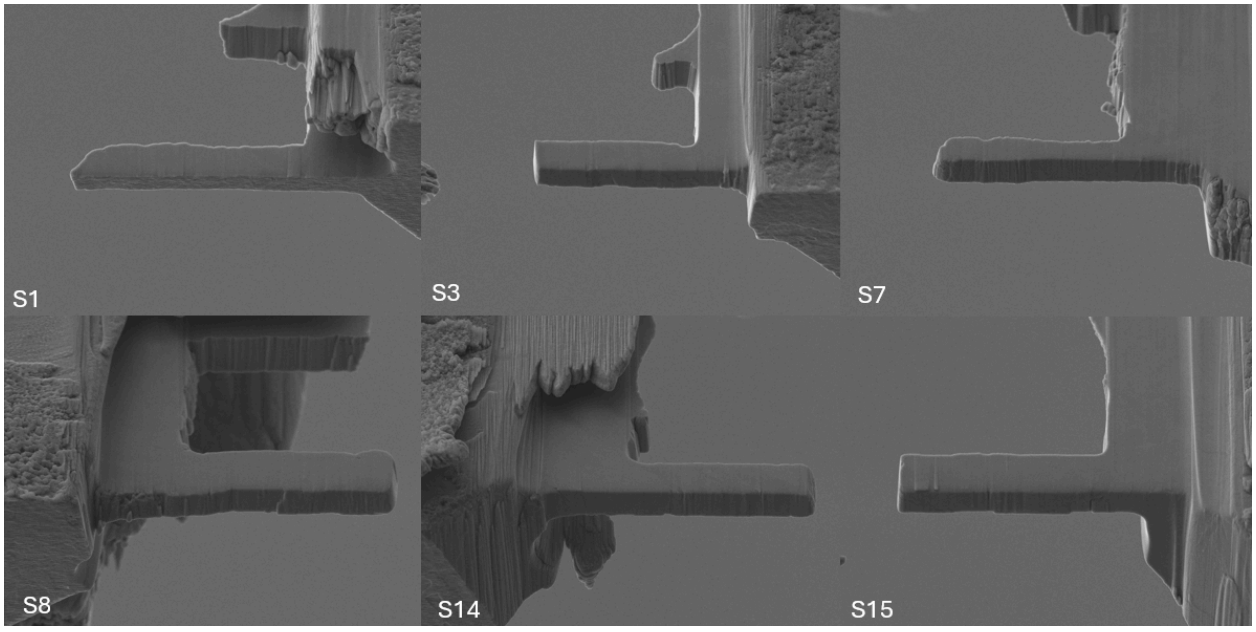

Figure 18. Final Images after the rough cutting of cantilevers

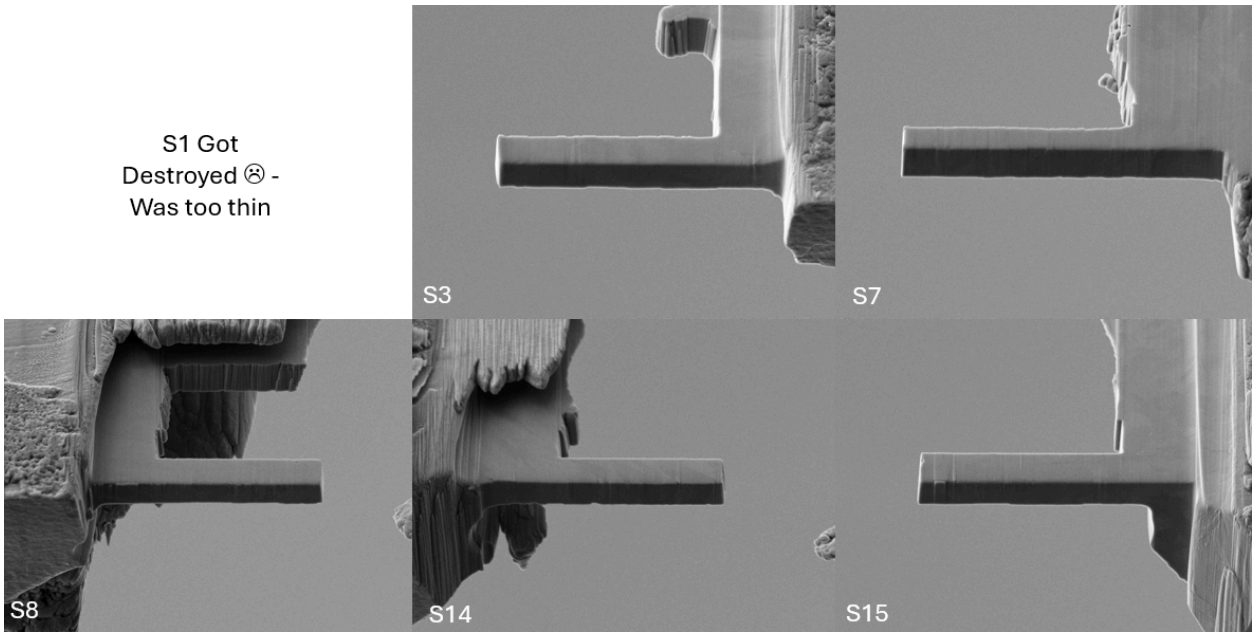

Figure 19. Final cantilevers before testing after fine polishing

The final cantilevers shown in Figure 19 are after the fine polishing step and right before the first round of testing using the uMS technique. It is noted that the sample denoted “S1" was destroyed during the fine milling phase of the machining due to misalignments of the FIB beam. The cantilevers were milled to an approximate size of 3x3x15 um however this varies from each

cantilever exactly. Precise measurements in the SEM were done to correlate the results in the end. It can be seen that the surface quality has improved drastically from the rough cutting step. However, certain artifacts of the FIB process can still be seen like the mild curtaining. These curtains are always present in FIB produced structures as certain features and grains will inevitably mill faster than others causing the lack of uniformity. This small difference is not expected to affect results in any significant manner. Now that the cantilevers were finished, the cantilevers moved onto testing using uMS.

2.3 Micromechanical Spectroscopy

Micromechanical spectroscopy (or uMS) was performed using the methodology stated in a previous section. This was done by loading the wedge specimen which held the cantilevers into a custom mount. This mount was subsequently loaded onto MUL's PI-85 picoindenter system which can be seen in Figure 20. This picoindenter system works by using an indenter tip mounted on parallel plate capacitors whose voltage can be used to read force values of the tip. A stage located within the PI-85 can then be moved in order to get accurate displacement values which can be correlated with the force of the indenter tip to give accurate load-displacement values. The system is also equipped to vibrate at specified frequencies which is integral to the uMS process. The papers by Alfrieder et al. give a great overview of this whole process as well as demonstrating this technique on other materials showing the quality and consistency of the data obtained [27, 28]. A primary difference between this study and prior ones done using this technique is the fact that a smaller amplitude and force was used for the contact load and load amplitude. During the testing of cantilever S7, it was found that the cantilever was slightly plastically deformed after the first round of testing which used a 500uN contact force and a 3uN load amplitude. Because of this, the cantilever was tested in a slightly bent state. Because we expect for the cantilevers to still be tested in an elastic manner, any amount of plastic deformation would not be optimal for data analysis and interpreting the results. Any amount of plastic deformation would nucleate many dislocations which would serve as an additional energy dissipation mechanism when analyzing the data. As a result of thai the contact load and load amplitude were lowered to 300uN and 1uN respectively to avoid this plastic deformation. This lower load condition did not cause any noticeable plastic deformation and was used for the rest of testing. It is also noted that sample "S3 " was accidentally destroyed during the testing due to a stage movement error. In total before heat treatment 4 samples were tested and labeled, S7, S8, S14 and S15. A total of 2-3 positions were sampled on each cantilever to gain consistency in the data and better statistics.

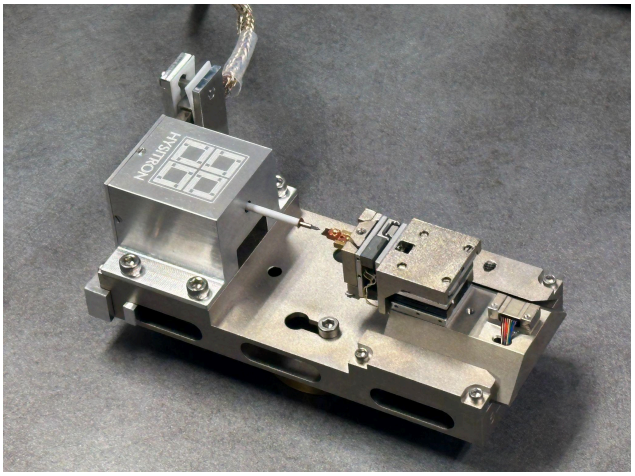

Figure 20. Hysitron PI-85 system used for the uMS cantilever testing with the wedge sample loaded inside.

Using the previously stated values of 300uN contact load, 1uN load amplitude, plus adding a dynamic frequency sweep from 200 to 300 Hz created the basic parameters for the experimental setup. Once the indenter tip was calibrated and setup was aligned so that the indenter tip was close to the cantilevers, the testing began. Close to the middle of the cantilever where resonance was expected to be found, the indenter tip was brought into contact with the cantilever and the testing began at the parameters stated above. SEM images during testing can be seen in Figure 21 and the raw data can be found in Figure 22. In total the testing took approximately 6 hours from start to finish to both insert/mount the specimen and test it.

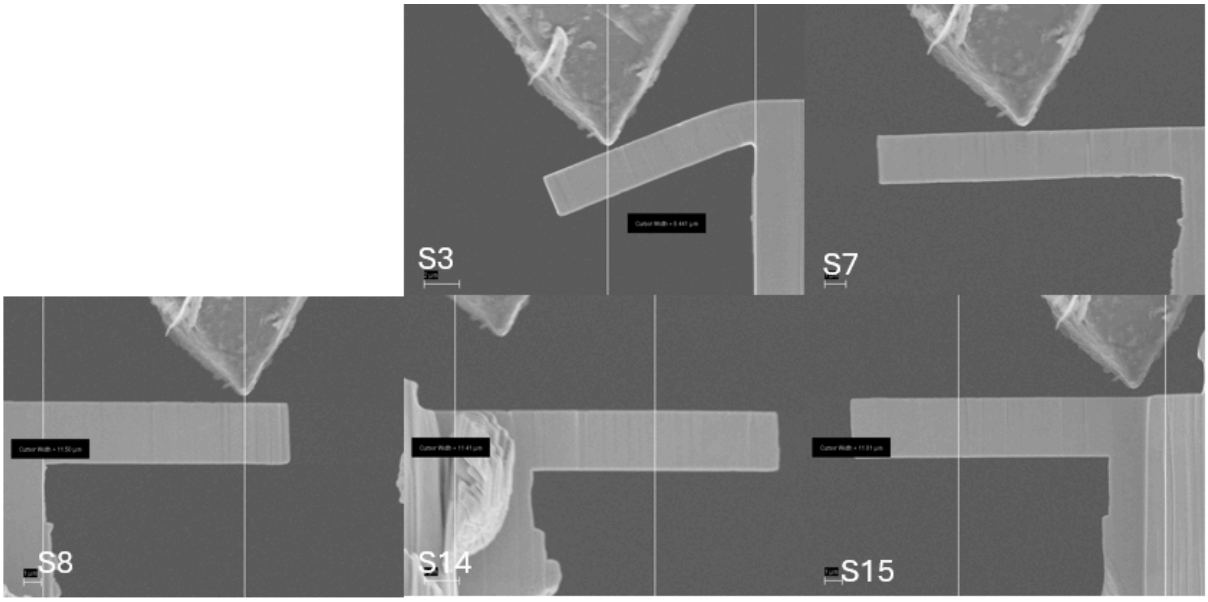

Figure 21. SEM images during the uMS testing. Note: the indenter tip (triangular shape on top) is not always depicted close to the testing position. Cantilever S8 accurately shows the position of testing.

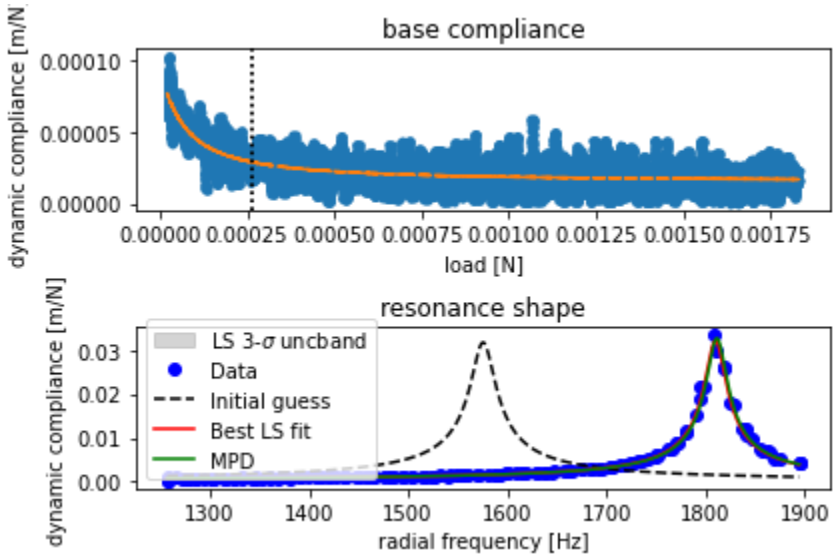

Figure 22. Raw data of the resonance peak of the S7 cantilever (top) shows the base compliance measurement (bottom) shows the resonance peak as well as the data analysis fitting of the curve.

The raw data which will be analyzed in the next section of the report shows two graphs. The top graph shows the base compliance of the system. This is essentially doing a similar frequency dependent measurement at the base of the cantilever on the same material, not on the cantilever. This data is used in order to correct for any error due to contact forces and to account for any part of the experiment which may have been influenced by factors other than the cantilever's mechanical properties. This data is used in the future data analysis and subtracted from the data to get the final data. The bottom graph shows the resonance frequency scan where in terms of radial frequency and dynamic compliance we can see the resonance shape. The code used to generate these plots was designed to use the emcee Markov chain monte carlo (MCMC) toolbox in python 3.8 to identify the resonance shape accurately from an initial guess.

2.4 Heat Treatment

The heat treatment (HT) occurred at a temperature of 750ºC for 1 hour using a vacuum furnace located at MUL. This vacuum furnace was run at an approximate vacuum pressure of 6E-5 mbar which should be sufficient to remove most oxygen and mitigate oxidation of the cantilevers. The ramping rate was around 10ºC/min and the specimen was air cooled back to room temperature before the next round of uMS testing. The chamber use for vacuum and heating can be seen in Figure 23 and shows the furnace setup. Due to potential issues with materials mismatch and diffusion, the sample had to be removed from its mount and the wedge specimen directly placed on a small steel foil plate to be inserted into the furnace.

Figure 23. Furnace setup for heat treating the F82H cantilevers.

Following the heat treatment no visible oxidation could be seen on the wedge specimen and the heat treatment seemed to have worked well. The sample was remounted and re-inserted into the SEM and PI-85 setup for further uMS testing after the heat treatment.

2.5 uMS Post-Heat Treatment

The same testing occurred after heat treating as before with the uMS testing. Sadly, specimen S15 was bent in between during the transfer of the pre-HT and post-HT testing so it was bent before testing meaning that post-HT data couldn't be extracted from this cantilever. There was an inevitable shift in angle of the specimen by around 1 degree due to the unmounting and remounting process however this is not expected to affect results. The cantilevers were tested using the same parameters and images and raw data can be seen in both Figures 24 and 25.

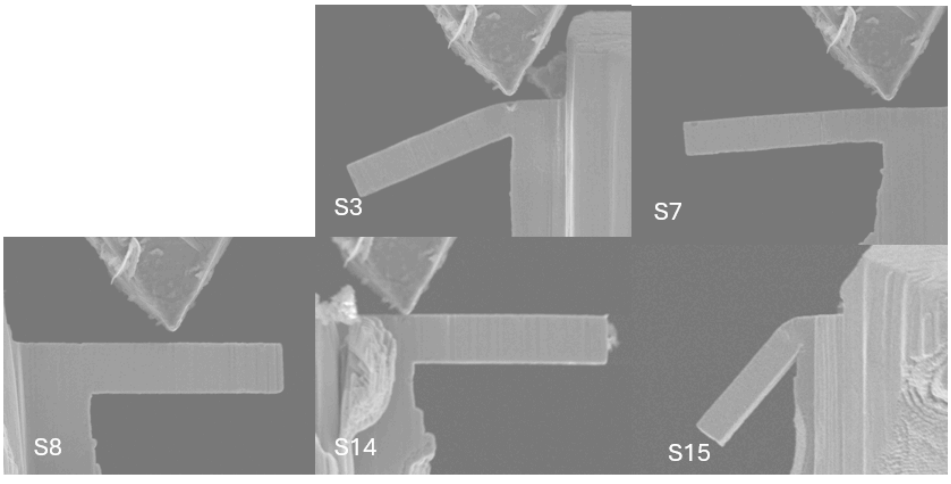

Figure 24. SEM images during the post-HT uMS testing. Note: the indenter tip (triangular shape on top) is not always depicted close to the testing position. Cantilever S8 accurately shows the position of testing.

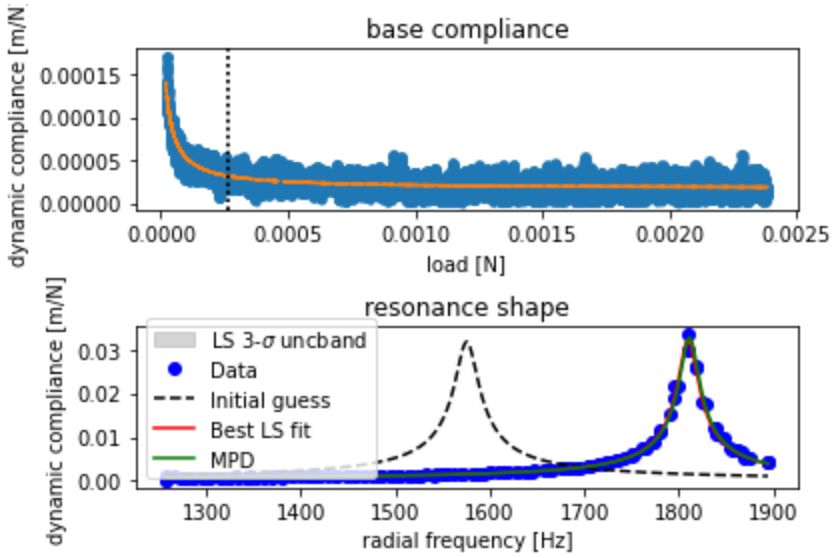

Figure 25. Raw data of the resonance peak of the post-HT S7 cantilever (top) shows the base compliance measurement (bottom) shows the resonance peak as well as the data analysis fitting of the curve.

The raw data shown in Figure 25 does not look significantly different from that of the pre-HT testing. The shift in the location of the resonance frequency is promising but, this peak location is also a function of distance along the cantilever so the small inconsistencies between the location of the previous testing and this testing can easily be attributed to this difference. The major difference in this data can be seen once empirical values of damping energy and youngs modulus start to be calculated which take these effects into consideration. During the testing nothing important of note took place and the testing seemed to have gone well and took a similar 4 hours of testing to finish.

3. Data Analysis

A python script was written to quantify the main important values of thai experiment. The two empirical values which can be extracted are the youngs modulus and the Q-inverse value. The youngs modulus can indicate a change in elastic properties which would be a very interesting finding for this system. Q-inverse on the other hand is the most important value gained from this experiment and it quantifies energy dissipation in the cantilever. The formula for Q-inverse and for the elastic/youngs modulus are as follows:

$$\frac{1}{Q} = Q^{-1} = \frac{1}{2\pi}\left(\frac{Energy\ Dissipated\ per\ Cycle}{Stored\ Energy}\right)$$

$$\frac{1}{Q} = \frac{Resonance\ Frequency}{FWHM}$$

$$E_{mod} = \frac{k_s L^3}{3I}$$

These values can be extracted from the resonance peak data and analyzed when compared with other cantilevers. The elastic modulus is calculated from first principals beam bending equations which only gives a rough estimate for the elastic modulus. The Q-inverse however is extremely accurate when accounting for the energy dissipation of the beam. Figure 26 gives a sense of how the data was analyzed from raw data to the analyzed data. Essentially the peaks were aligned to a normalized frequency and the compliance was normalized to account for the different deflections of the beam at different load conditions.

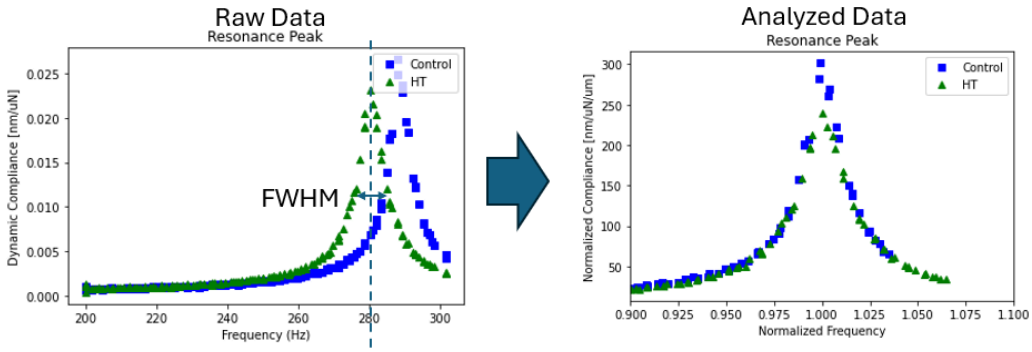

Figure 26. Raw to analyzed data conversion with FWHM and resonance frequency noted.

This process of data analysis was automated within python 3.8 and the results are shown in Figure 27. In total the first 5 tests on cantilevers: S3, S7, S8, S14 and S15 are shown. It is noted that S1 was lost during FIB milling, S3 was pre deformed and not very suitable for testing, and S15 post-HT data was not able to be measured due to the sample breaking between the testings. The various Q-inverse values and the microstructural features are shown in Figure 28.

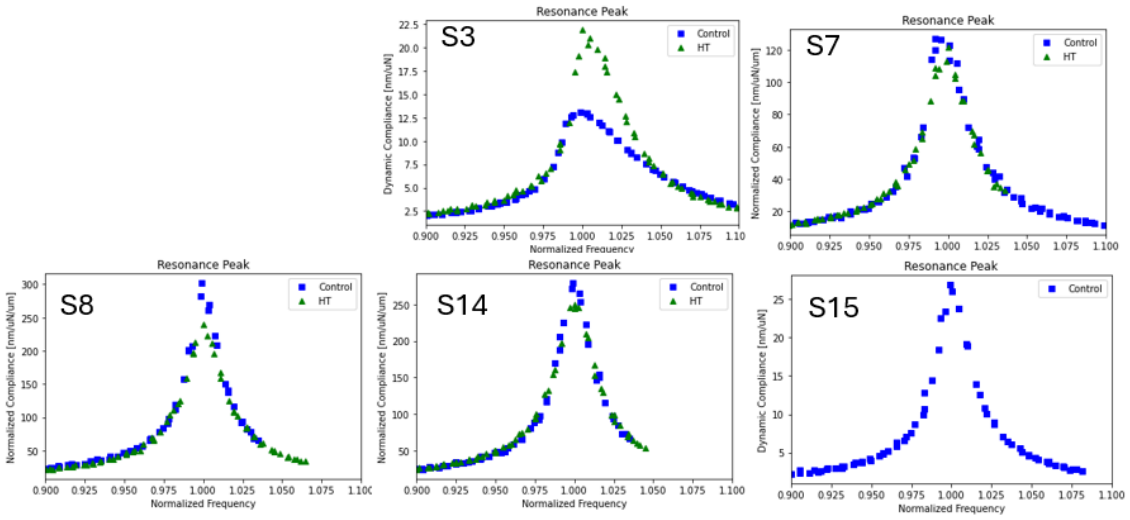

Figure 27. Analyzed data for all 5 cantilever specimen produced plotting normalized compliance and normalized frequency showing resonance peak

Cantilever ID	Cantilever Microstructure	Q-Inverse Pre-HT	Q-Inverse Post-HT	ΔQ-Inverse	Energy Dissipation
S3	High Angle Grain Boundary	0.0345	0.0210	-0.0135	High Energy Dissipation Decrease
S7	High Angle Grain Boundary – Block Boundary	0.0169	0.0187	+0.0018	Highest Energy Dissipation Increase
S8	Lath Martensite	0.0147	0.0151	+0.0004	Lowest Energy Dissipation Increase
S14	45 Degree Oriented Lath Martensite	0.0150	0.0160	+0.0010	Medium Energy Dissipation Increase
S15	High Angle Grain Boundary	0.0141	-	-	-

Figure 28. Q-Inverse values for each cantilever and microstructural feature before and after HT

Analyzing the data one by one we find some interesting findings from this study. S3 which encapsulated a HAGB had the only case where the energy dissipation capabilities of the cantilever decreased. While this is puzzling at first, when you consider the fact that the cantilever was pre-deformed before testing we can see why this result occurred. A primary energy dissipation mechanism for this form of testing is through dislocations which heavily contribute to the observed Q-inverse. Before heat treating, the high Q-inverse already indicates that there is another energy dissipation mechanism at play which is giving such a high internal friction. Recalling from before where plastic deformation nucleates lots of dislocations, we can see that

the large amount of dislocations resulting from the accidental plastic deformation caused a vast increase in energy dissipation of the cantilever. However after heat treating much of these dislocations were annealed out of the system causing the only decrease in Q-inverse observed. While this result is not publishable due to the complex stress state which would be hard to correlate and the many unknowns once deviating from classical beam bending formulas, it is a promising result which shows the capabilities of the technique.

S7 on the other hand shows the expected energy dissipation increase after the heat treatment. The high angle grain boundary shows a higher amount of energy dissipation when compared to the lath martensite cantilevers. However after the heat treatment this value increases even more. However if the mechanism was purely through dislocation annealing, then we would see the same result as what was seen with S3 with a decrease in energy dissipation, however this increase indicates that some other phenomenon is occurring. The other known phenomenon which can be attributed to this increase is the nucleation of precipitates on the grain boundaries. The carbides which nucleate should increase the energy dissipation.

S8 and S14 both show similar trends to that of S7 with an increase in energy dissipation as evidenced by the Q-inverse. However we can see that the energy dissipation increase is not as high when compared to that of S7. This potentially means that the lath structure of martensite does not have as high energy dissipation capabilities as high angle grain boundaries. On top of this, after a heat treatment, the difference in Q-inverse is not as high as with S7. This would indicate that carbides do not preferentially nucleate on the martensitic laths. In addition the 45 degree oriented martensite has a greater increase in energy dissipation compared to oriented martensitic laths. The S15 cantilever was broken during testing so post HT data was not gained for this sample.

4. Future Work & Improvements

While this data looks promising the lack of statistics is not optimal for this experiment. While it is almost never a goal of any micromechanics experiments to gain large statistics of a phenomenon, a larger amount of samples tested would only serve to bolster our claims on carbide interactions. Also the extremely small increases in Q-inverse of these samples further highlights a need for future experimentation.

The next steps for this project will include correlating these Q-inverse values to actual energy dissipation mechanisms relating to the individual microstructure of each sample. Every cantilever will need to be analyzed one by one to get a sense of why the unique microstructure of each contributes to the Q-inverse value. The main sources of damping in these cantilevers are thermoelastic, dislocation based, defect based (i.e. grain boundaries), and other minor sources like air damping. The effect of each of these damping mechanisms on the measurements for the Q-inverse of the cantilevers will need to be thoroughly analyzed before publication.

4. Conclusion

This project aimed to quantify carbide interactions at grain boundaries within the ferritic martensitic steel F82H. In total, 5 cantilevers were produced and tested using the novel micromechanical spectroscopy method. Data was recorded before and after heat treatment.

Two future papers are planned for this project. One aimed at being submitted in October 2024 whose scope encompasses the initial measurements of grain boundary characterization and the damping measurements. The second paper is planned for characterizing the effect of heat treatment on the damping capabilities of the cantilevers and correlating tht with the grain boundary orientations.

References

1. Inc G (2016) Gallup Vault: Nuclear Power Plant Fears After Chernobyl. In: Gallup.com. https://news.gallup.com/vault/191099/gallup-vault-nuclear-power-plant-fears-chernobyl.aspx. Accessed 30 Jul 2024
2. Climate goals call for speedier expansion of nuclear power - World Nuclear News. https://www.world-nuclear-news.org/Articles/Climate-goals-call-for-speedier-expansion-of-nucle. Accessed 22 Jul 2024
3. Energy Production and Consumption in the United States | EBF 301: Global Finance for the Earth, Energy, and Materials Industries. https://www.e-education.psu.edu/ebf301/node/457. Accessed 22 Jul 2024
4. First new U.S. nuclear reactor since 2016 is now in operation - U.S. Energy Information Administration (EIA). https://www.eia.gov/todayinenergy/detail.php?id=57280. Accessed 30 Jul 2024
5. What is ITER? In: ITER. http://www.iter.org/proj/inafewlines. Accessed 22 Jul 2024
6. Krane K (1987) Introductory Nuclear Physics. Wiley and Sons
7. Morse E (2018) Nuclear Fusion, 1st ed. Springer International Publishing
8. Plot of Binding Energy per Nucleon against Mass Number - Important Conclusions. https://www.conceptualphysicstoday.com/2017/12/plot-of-binding-energy-per-nucleon.html. Accessed 22 Jul 2024
9. History of Fusion. In: EUROfusion. https://euro-fusion.org/fusion/history-of-fusion/. Accessed 22 Jul 2024
10. (2021) ITER Talks (1): Introduction to ITER
11. Allen T, Busby J, Meyer M, Petti D (2010) Materials challenges for nuclear systems. Materials Today 13:14–23. https://doi.org/10.1016/S1369-7021(10)70220-0
12. ITER Members. In: ITER. http://www.iter.org/proj/countries. Accessed 22 Jul 2024
13. Kawamura Y, Gwon H, Guan W, et al (2020) Progress of water cooled ceramic breeder test blanket module system. Fusion Engineering and Design 161:112050. https://doi.org/10.1016/j.fusengdes.2020.112050
14. Kawamura Y, Hirose T, Guan W, et al (2024) Overview of progress on water cooled ceramic breeder blanket in Japan. Fusion Engineering and Design 201:114260. https://doi.org/10.1016/j.fusengdes.2024.114260
15. Someya Y PROGRESS IN DESIGN AND ENGINEERING ISSUES ON JA DEMO
16. (2021) ITER Talks (2): The ITER Blanket System
17. Was G (2007) Fundamentals of Radiation Materials Science. Springer Berlin Heidelberg,

Berlin, Heidelberg
18. Henry J, Maloy SA (2017) Irradiation-resistant ferritic and martensitic steels as core materials for Generation IV nuclear reactors. In: Structural Materials for Generation IV Nuclear Reactors. Elsevier, pp 329–355
19. Cabet C, Dalle F, Gaganidze E, et al (2019) Ferritic-martensitic steels for fission and fusion applications. Journal of Nuclear Materials 523:510–537. https://doi.org/10.1016/j.jnucmat.2019.05.058
20. Fusion power plant alloys. https://www.phase-trans.msm.cam.ac.uk/2006/Irradiated_Steel/Irradiated_Steel.html. Accessed 22 Jul 2024
21. zz_hugo (2020) Long-lived Fission Products. In: radioactivity.eu.com. https://radioactivity.eu.com/nuclearenergy/long_lived_fission_products. Accessed 22 Jul 2024
22. Callister W, Rethwisch D (2007) Material Science and Engineering – An Introduction
23. Ostrovski O, Belashchenko D (2013) Thermophysical properties and structure of liquid Fe-C alloys. High Temperatures - High Pressures 42:137–149
24. Time-Temperature-Transformation (TTT) Diagram | Metallurgy for Dummies. https://www.metallurgyfordummies.com/time-temperature-transformation-ttt-diagram.html. Accessed 22 Jul 2024
25. (2011) Martensitic transformation
26. A simple model of solid matter - Nexus Wiki. https://www.compadre.org/nexusph/course/A_simple_model_of_solid_matter. Accessed 22 Jul 2024
27. Alfreider M, Issa I, Renk O, Kiener D (2020) Probing defect relaxation in ultra-fine grained Ta using micromechanical spectroscopy. Acta Materialia 185:309–319. https://doi.org/10.1016/j.actamat.2019.12.011
28. Alfreider M, Meindlhumer M, Ziegelwanger T, et al (2024) Revealing dynamic-mechanical properties of precipitates in a nanostructured thin film using micromechanical spectroscopy. MRS Bulletin 49:49–58. https://doi.org/10.1557/s43577-023-00549-w